Increased hot electron production from the addition of a gas cell in sub-picosecond laser-foil interactions

T.Peterken, A.P.L.Robinson, R.M.G.M.Trines and R.J.Clarke

Published version information

Citation: T Peterken et al. 'Increased hot electron production from the addition of a gas cell in sub-picosecond laser–foil interactions.' Physics of Plasmas, vol. 27, no. 12 (2020): 123101.

DOI: 10.1063/5.0021221

Increased Hot Electron Production from the Addition of a Gas Cell in Sub-Picosecond Laser-Foil Interactions

T.Peterken,[1] A.P.L.Robinson,[1, a)] R.M.G.M.Trines,[1] and R.J.Clarke[1]
Central Laser Facility, STFC Rutherford-Appleton Laboratory, Didcot, OX11 0QX, United Kingdom

A number of recent experiments at the VULCAN laser at the Rutherford Appleton Laboratory involving high intensity (10^{19}W/cm^2) sub-picosecond laser pulses incident on thin ($\sim 10\mu$m) metal foils for use as a proton probe have suggested that the addition of a gas cell behind the foil results in a significant increase in the production of hard x-rays, particularly in the direction counter to the incident laser direction. In this paper we consider two mechanisms that might contribute to to this effect. Analysis of these two mechanisms indicate that there are plausible physical mechanisms that could give rise to the observations, and thus the physics of these gas-cell targets merits further study.

I. INTRODUCTION

There has been considerable recent interest in the use of ultra-intense laser-plasma interactions to provide a source of x-rays, both from the betatron mechanism in gas jet interactions[1] and from solid targets[2]. This is driven by the potential that these new x-ray sources might find imaging applications in high-value commercial areas such as the aerospace, nuclear, and advanced manufacturing sectors. In the case of solid targets, the x-ray production is attributed to fast electron propagation through a sufficiently thick high-Z bremsstrahlung convertor[3], and improving these sources will, in part, depend on how the collective understanding of fast electron generation and phenomena develops.

Recently, experiments conducted at the VULCAN laser facility (Target Area West) at the Rutherford Appleton Laboratory, using thin foil targets with the rear surface in contact with a gas cell, have raised suspicion that the addition of the gas (or potentially the target geometry to achieve this) results in a significant increase in the production of hard (>100keV) x-rays able to exit the interaction chambers. Similar gas cells have been used in a number of prior experiments[5,7,8]. Figure 2 shows the radiation dose internal to the experimental area averaged over the experimental periods. These measurements are made with passive Luxel+ environmental monitors from Landauer using a combination of Optically Stimulated Luminescence (OSL) detectors for photon measurements between 5keV and 6MeV and an in-built Neutrak CR39 detector for neutron measurements. The monitors are located about 5m away from the interaction point in the interaction chamber.

Doses within the area are derived from the short pulse interactions which are typically thin (10's microns) high z (typically gold) targets mounted directly onto plastic or metallic stalks, used for the generation of proton beams for probing the plasma interactions. Although each experimental campaign is different, we have generally observed similar doses for thin target experiments since there is very little bremsstrahlung conversion in such thin targets. Typical doses for this type of experiment are in the order of 0.1 - 0.2mSv (a). Occasionally thick target experiments take place to generate a burst of high-energy radiation for imaging experiments using mm thickness high z targets to optimise bremsstrahlung production (b) or where secondary targets are used close to the primary target (for example proton-neutron converters) resulting in the same effect of an increased bremmstrahlung.yield

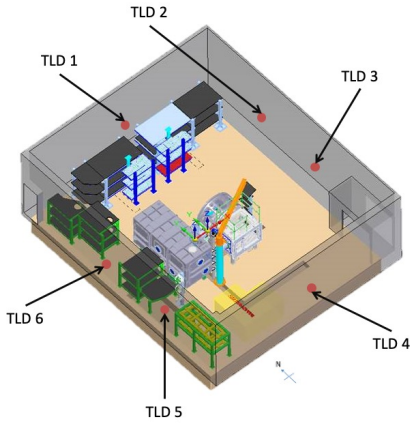

FIG. 1: A schematic illustrating Target Area West, showing the position of the six Landauer monitors (denoted TLD).

a)corresponding author, email : alex.robinson@stfc.ac.uk

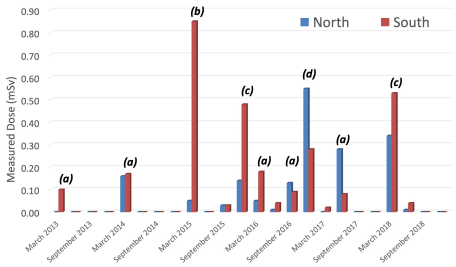

FIG. 2: Radiation doses detected in target areas over several experimental periods (dates given). Measurements labelled (a) correspond to typical experimental campaigns not expected to produce exceptional doses of hard-xrays. Measurements (b) and (d) correspond to experimental campaigns that were expected to produce high hard x-ray yields, and measurements (c) correspond to campaigns involving gas-cells. For details see text.

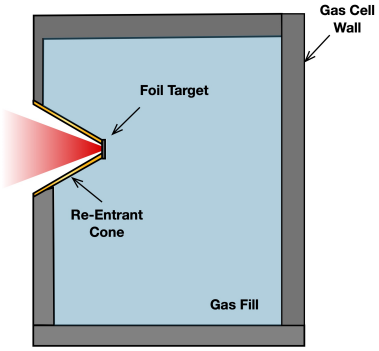

FIG. 3: A schematic illustrating the key features of the gas cell target.

due to the electron interactions in this second target.

However, when the gas fill is introduced behind target (c) the rearward dose not only peaks significantly above normal expectations, but is also significantly higher than the forward direction. It should be noted that the same effect is not observed using a gas fill where gas is also present at the front surface of the target. However, potential detrimental effects on the beam focussing also have to be considered when considering a gas fill geometry and the impact on the resultant electron generation. Obviously the amount of data in this analysis is insufficient to draw a firm conclusion, however suggestive it might be, and it is for this reason that we carried out the theoretical study reported herein, which we believe justifies a more in-depth experimental investigation.

The gas fill was introduced behind the foil target by using a gas cell. The gas cell is relatively large (on the order of 10cm in each dimension, up to about 50cm for some gas cell designs), with thick metallic walls (1–2 cm thick). A very small area of the foil target is accessible at the apex of a re-entrant cone (typically 2–3mm). The laser is focussed on the apex of the re-entrant cone where the front side of the foil is exposed. This is shown in the illustration in fig. 3, in which we provide a schematic illustration of a portion of the gas cell target. As indicated in fig. 3 the rear of the foil is directly in contact with the gas fill. Foils were typically 10 μm thick, and usually composed of Fe (or Fe-based alloys), Cu, Al, or Au. The re-entrant cone was large enough to admit the focussing of the laser by the F3 focussing optic, i.e. opening angle larger than 20°.

If an effect is present, then it is most likely the case that some aspect of the target design results in either (a) a substantial increase in the number of hot electrons, and/or (b) a substantial alteration in the angular distribution of the hot electrons. In this paper we have investigated two mechanisms that each achieve one of these. The first mechanism is that of the basic absorption mechanism in this interaction, where we find, under certain circumstances, that there are more high energy backward propagating electrons than forward propagating electrons of the same energy. The second mechanism is a mechanism whereby the sheath field at the foil-gas interface can draw in and accelerate cold electrons from the gas leading to an increase in the number of hot electrons. The paper is thus structured as follows:

1. In Section II we discuss aspects of x-ray generation via bremmstrahlung and how this relates to the faste electron properites.

2. In Section III we present 2D PIC simulations of the laser-foil interaction. Note this is the laser-foil interaction alone without accoutning for the gas fill. Even without this, the features of the angular distribution of the fast electrons might account for the observed differences in x-ray emission.

3. in Section IV we then discuss the sheath mechanism of hot electron multiplication

4. Finally, in Section V we present the overall conclusions of this study.

II. HOT ELECTRONS AND X-RAY PRODUCTION

The first quantitative consideration is the electron energies required to produce > 100KeV x-rays. The x-ray spectrum caused by high energy electrons passing

through a material is given by Kramer's law[11]:

$$I(\lambda) \propto \frac{1}{\lambda^3}\left(\frac{\lambda q W_i}{hc} - 1\right) \tag{1}$$

where W_i is the kinetic energy of the incident electron in electron volts (reserving E for electric field strength and T for temperature). A 100KeV photon corresponds to a wavelength of[12] $\lambda = \frac{hc}{W_p q} \sim 10^{-11} m$. Even though the electrons emit a continuous spectrum, it would be useful to count only those electrons that release 85% − 90% of their energy in photons > 100KeV. The smallest wavelength possible from a highly relativistic electron is, via energy conservation, $\lambda_{min} = \frac{hc}{qW_i}$ and hence from λ_{min} it is easy to compute a relevant electron energy cut off.

$$\frac{\int_{\lambda_{min}}^{10^{-11}m} \frac{1}{\lambda^3}\left(\lambda/\lambda_{min} - 1\right) d\lambda}{\int_{\lambda_{min}}^{\infty} \frac{1}{\lambda^3}\left(\lambda/\lambda_{min} - 1\right) d\lambda} \approx 0.88. \tag{2}$$

This solves to get a minimum electron kinetic energy of $\sim$ 2MeV. We can compare this energy to the characteristic energies expected for the hot electrons in relativistically intense laser-solid interactions. For example, the 'ponderomotive' scaling given by Wilks is:

$$E_{pond} = m_e c^2 \left[\sqrt{1 + \frac{I_L \lambda^2}{1.38 \times 10^{18} \mathrm{Wcm}^{-2} \mu m^2}} - 1\right]. \tag{3}$$

According to the scaling of Wilks, this means that the characteristic hot electron energy will exceed 2 MeV when $I_L > 3.2 \times 10^{19}$ Wcm^{-2} (assuming 1μm wavelength). So laser-solid interactions at intensities available with the VULCAN laser (which substantially exceed this threshold) should produce a copious number of electrons above 2 MeV. This statement is quite consistent with many years of experimental studies on this laser system. It thus seems unlikely that any increase in x-ray production is due to changes in the characteristic energy of the hot electrons, and it would therefore appear to be the case that the effect of the gas cell, if any, would be to : (a) substantially increase the number of hot electrons, and/or (b) substantially alter the angular distribution of the hot electrons, as stated earlier.

Once a model has determined by electron distribution function, the ratio of the backward to forward x-ray signals can be estimated by assuming that all electrons propagate through an equal thickness of high-Z material. Using Eq. 1, this simple estimate becomes,

$$\frac{S_b}{S_f} = \frac{\int_{bkwd.} f_e(\gamma - \gamma_{min}) d^3\mathbf{p}}{f_e(\gamma - \gamma_{min}) d^3\mathbf{p}}, \tag{4}$$

where $(\gamma_{min} - 1) m_e c^2$ is the minimum electron energy described above, and bkwd. and fwd. indicate integration over the foward and backward pointing regions of phase space.

Run	n_{slab}	l_{slab}	Z/A	a_0	Notes
BL	60	5	1	5	Baseline case
A	30	5	1	5	
B	10	5	1	5	
C	60	5	1	5	tilted
D	60	20	1	5	thicker
E	60	5	1	3.54	half intensity
F	60	5	1	7.07	double intensity
G	60	5	1	5	with L=10 linear ramp on front
H	60	5	1/2	5	
I	30	5	1/2	5	
J	10	5	1/2	5	
K	60	20	1/2	5	thicker
L	60	5	1/2	3.54	half intensity
M	60	5	1/2	7.07	double intensity
N	60	5	1/2	5	tilted

TABLE I: Values of parameters used in 2D PIC simulations.

III. 2D PIC SIMULATIONS OF LASER-FOIL INTERACTION

A. Setup

Two dimension (2D) Particle-in-Cell (PIC) simulations were carried out to study the laser-foil interaction using the OSIRIS code[30]. In these simulations, this was studied without the gas fill being present, as it was not obvious that the gas fill would significantly influence the actual generation of fast electrons at the front surface. Additionally, we did not include the re-entrant cone in this simulation as the area of exposed foil is much larger than the focal spot size. Thus the simulation model was reduced to that of a laser pulse interacting with a simple slab. These simulations were carried out on a 6000 × 6000 cell grid with a total size of 188.5 × 188.5 $(c/\omega_L)^2$. The baseline target is a rectangular slab, which is centred on (100.0, 94.25)(c/ω_L), with thickness $l_{slab} = 5.0$ (c/ω_L), and width 160.0 (c/ω_L). In the baseline case this slab consists of electrons and protons each at a uniform density of $n_{slab} = 60\ n_c$ (thus the slab is initially neutral). A linearly polarized laser pulse (polarized in the y direction) propagates parallel to the x-axis, centred on y =94.25 (c/ω_L). The pulse has a trapezoidal temporal profile with a linear rise and fall over 25 ω_L^{-1} and a central constant region over a 300 ω_L^{-1} duration. The focus is set at $x = 100(c/\omega_L)$, with a spot radius of $3(c/\omega_L)$ and an a_0 =5. Simulations were typically run up to a time of 228 ω_L^{-1}. In dimensional units, if a laser wavelength of 1μm is assumed, the box size is 30×30 μm, the laser pulse duration is around 160 fs, and simulations are run up until 120 fs.

The set of simulations carried out and the specific parameters are tabulated in Table I.

Where we have denoted a simulation as being tilted,

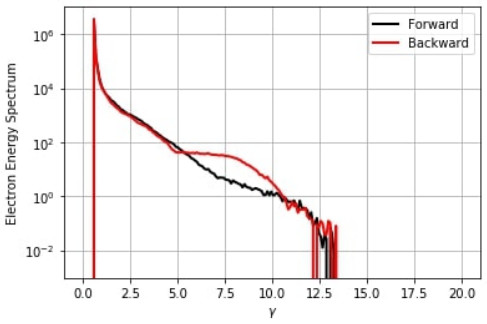

FIG. 4: Plot of forward and backward going electron spectra in run BL at $228\omega_L^{-1}$

Run	Higher Backward Flux?	γ range	S_b/S_r
BL	Y	5–9	1.57
A	Y	6–9	0.71
B	Y	6–10	0.76
C	Y	> 5	. 0.78
D	N	n/a	0.47
E	Y	5–7.5	2.31
F	Y	> 9	0.73
G	N	n/a	0.49
H	Y	> 5	1.63
I	Y	5–10	1.22
J	Y	5–10	1.21
K	Y	> 7.5	0.57
L	Y	> 4	3.81
M	Y	> 5	0.95
N	Y	> 5	1.06

TABLE II: Summary of observations of greater backward electron flux in 2D PIC simulations.

the angle of incidence is 10°.

B. Results and Discussion

The electron distributions from these simulations were analyzed, and it was found that there were substantial differences between forward and backward going electrons. A typical example of this is the baseline (BL) simulation. The spectra of forward going ($p_x > 0$) and backward going ($p_x < 0$) are plotted in fig. 4. Note that the electron spectra are calculated by taking all of the electrons in the simulation box at the time stated, and only splitting into 'forward' and 'backward' by $p_x > 0$ and $p_x < 0$ respectively.

As can be seen in fig. 4 there is a very significant energy region where there are many more electrons in the backward direction than in the forward direction. In the specific case of the baseline simulation this runs from around $\gamma = 5$ to just over $\gamma = 10$ (approximately 2MeV to 4.5MeV). Below this the two spectra overlap, although only electrons over 2MeV are relevant, and above this the two spectra overlap. These results are quite typical of what we observe in many of the simulations listed in Table I, however this is not true in every single case. In table II we have tabulated our observations indicating in which simulations we observe these regions where there is greater backwards electron flux and what the energy range is. The estimated ratio of the backward to forward x-ray flux due to electron emission is also included. This ratio is calculated by using Eq. 4, but with the integration carried out over the two available momentum directions of the simulation outputs only, and only over a cone half-angle of 45°. The latter change was done to account (to some extent) for the very high angle electrons not contributing much to the detectable forward/backward signals.

Let us comment on the trends seen in table II. Firstly, the occurrence of a significant region in the energy spectrum where is higher backward than forward flux is very common in this set of simulations. There are only two simulations out of 15 where this is *not* observed, so the feature shown in fig. 4 is ubiquitous in this set of simulations. The estimated ratio of the x-ray fluxes is a different matter, as the occurrence of this spectral region is not a guarantee that the backwards x-ray flux will be higher (at least in the way we have estimated the x-ray signal ratio here). However we can discern three trends:

- The backward-to-forward ratio of x-ray signal is higher for a higher slab density : look at the trends in A–C and H–J
- The backward-to-forward ratio of x-ray signal appears to be favoured by somewhat lower laser intesity than in the baseline case : look at cases E and L.
- The backward-to-forward ratio of x-ray signal appears to be higher for the cases where Z/A = 1/2, rather than 1 : see A–F versus H–N

Importantly, from the entire set of simulations, there are a number of simulations where the estimated ratio of backard-to-forward x-ray signal is highly consistent with the data that has been gathered thus far. The observed ratio of unusual x-ray doses ranges from 1.5 to 3.2. Amongst our results we find that when the estimated backward signal is greater the ratios range from 1.06 up to 3.8, which completely covers the range that has been observed experimentally. Therefore it is possible that the generation of a higher flux of backward going fast electrons alone could explain the observations, just due to the nature of the laser-plasma interaction.

We should comment on some of the trends that are not stated in table II. Firstly we note that the strength of the effect (the extent to which the number of backward going electrons is greater than the forward going ones at

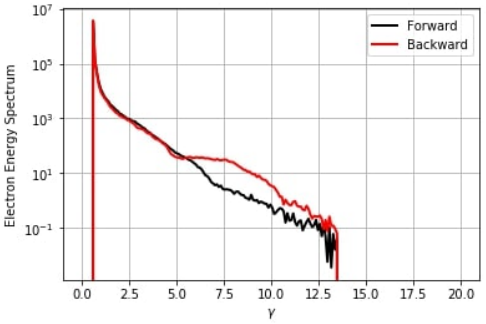

FIG. 5: Plot of forward and backward going electron spectra in run H at $228\omega_L^{-1}$. Run H is identical to the BL run except that $Z/A = 1/2$.

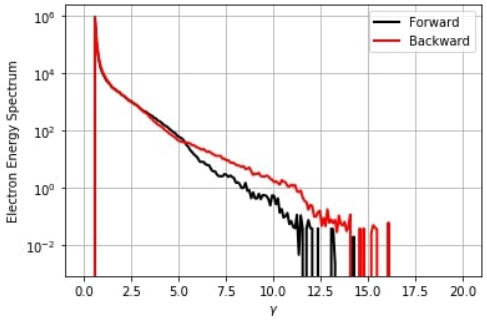

FIG. 6: Plot of forward and backward going electron spectra in run C at $228\omega_L^{-1}$. Run C is identical to the BL run except that the target is tilted to give a 10° angle of incidence.

any given energy) is stronger at higher n_{slab} than lower n_{slab}. Secondly the effect appears to be slightly stonger the lower Z/A is for the slab ions. For example the spectra for run H are shown in fig. 5. This means that the $Z/A = 1$ results will tend to underestimate the production of backward going electrons compared to many 'real' targets as for most elements $Z/A = 1/2$ at full ionization. Thirdly the tilted targets have an angle of incidence of 10°, however even this small angle of incidence results in a noticeable increase in the strength of this effect. For example, the spectra for run C are shown in fig. 6. Since most experiments are done with some angle of incidence, this suggests that simulations done at normal incidence will underestimate this effect in comparison to more 'realistic' configurations. The only change to the baseline configuration that was seen to reduce or remove this effect, with some consistency, was the addition of a smooth density profile on the front of the slab (e.g. run G), which is a change normally associated with laser prepulse. Increasing the target thickness has some disruptive effect, but is not very consistent when other factors are changed, e.g. run D vs run K. However some further comments need to be made on this point. The first being that we have not been able to exhaustively study all possible configurations. The second is that in experiments with relatively long pulses, e.g. 500fs compared to those with less than 100fs duration, that there may be a steepening effect due to the pondermotive force which effectively restores the sharp density gradient. This could be elucidated by extending the present study to somewhat greater times and pulse durations, which has not been done so far because of the computational expense involved.

Alongside the energy spectra, there are very substantial differences between forward and backward going electrons in terms of the angular distributions. In fig. 7 we show the angular distributions in two energy ranges in the BL simulation. Although both forward and backward distributions appear to bimodal, the positions and widths of the peaks do not coincide. This suggests that the mechanisms generating the forward and backward electrons have certain crucial differences.

There is also the question of what mechanism(s) lead to the observations made in the simulation outputs? In the baseline simulation we do observe the production of bunched electrons. There is also the importance of a steep density gradient on the front surface, and these two factors suggest that a mechanism that is closely related to Baeva's Zero Vector Potential (ZVP)[26,27] mechanism is at least partially responsible for these observations. A key part of the ZVP mechanism is that electrons are initially accelerated outwards into the vacuum, against the incoming laser direction, so this mechanism (or something very similar) can provide an initial injection of energetic electrons backwards into the vacuum. In fig. 8 p_x-x phase space plots from the BL simulation are shown at different times. The strong bunching of the electrons can be seen in these plots. At early times the maximum forward momentum of electrons generated at the front surface is $\approx 5m_ec$, and this appears to increase due to recirculation in the foil (up to around 15–20 m_ec). We also observe that the backward going energetic electrons have a large angular spread (see fig. 7). This suggests another mechanism is acting, and we posit Direct Laser Acceleration (DLA) to be the second mechanism. It has been shown[29] that a defocussing pulse is able to provide net energy gain to single electrons, whereas a focussing pulse cannot. Thus further acceleration of the ejected electrons can be provided by the defocussing reflected wave, which thus also accounts for the considerable angular spread of these electrons. In the phase plots of fig. 8 there is strong evidence for DLA. On examining fig. 8 (b) and (c) we see that on the non-irradiated side of the slab the maximum forward momentum of the electrons decreases as one moves away from the foil. On the front

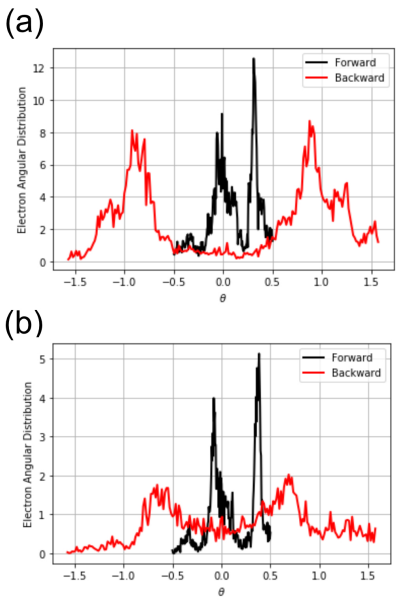

FIG. 7: Angular distribution of electrons in (a) $6< \gamma <6.5$ range, and (b) $7.5< \gamma <8.0$ range in BL simulations at $228\omega_L^{-1}$.

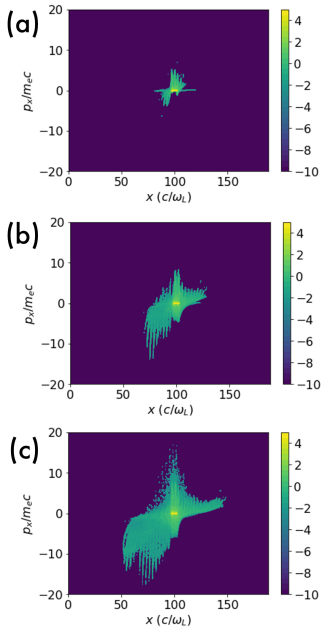

FIG. 8: p_x-x phase space plots ($\log_{10}$) from the BL simulation at (a) 124.2 ω_L^{-1}, (b) 144.9 ω_L^{-1}, and (c) 165.6 ω_L^{-1} .

side of the foil, we see that the maximum backward going momentum *increases* on moving away from the foil. This indicates that electrons are being accelerated backwards in the 'vacuum' region some distance from the foil, which is a very strong indication that DLA is responsible. It would also appear from these plots that DLA is responsible for up to $\approx 10 m_e c$ of backward momentum. Thus the high fluxes of backward going fast electrons observed in these simulations has a reasonably plausible explanation in terms of the combined action of the ZVP mechanism and DLA.

Now, so far this explanation has not invoked the role of gas cell at all. Let us now examine the link. The gas cells used in these VULCAN experiments change the experimental configuration from prior experiments in several respects, as shown in fig. 3. Obviously there is the gas behind the proton-probe foil, but the gas cell housing also introduces a thick volume of metal around the gas, and immediately adjacent to the proton-probe foil. The laser is brought to the foil through a re-entrant conical path through the metallic shell, with only a small area of exposed foil at the apex of this path. If the interaction thus produces a significant number of backward going fast electrons with a substantial angular spread, then many of these electrons can enter the metal shell which will then act as a proximate x-ray convertor. Thus the nature of the gas cell housing or shell acts to create the strong backward x-ray flux in this case.

IV. SHEATH MECHANISM OF HOT ELECTRON MULTIPLICATION

A. Theory

We now turn our attention to the second mechanism that we considered, namely the possibility of a sheath field at the foil-gas boundary producing a growth in the number of fast electrons. We envision this working as follows : As the electrons travel through the foil and exit through the foil-gas boundary, the resulting charge imbalance causes an electrostatic sheath field to be set up[18,19]. The presence of the gas will reduce the capability of the sheath to reflect the fast electrons, but the

sheath will accelerate electrons from the gas to high energy, which thus generates new fast electrons, and thus might be termed a 'multiplication' mechanism. The effectiveness of this mechanism will depend on the gas density being somewhat less than the fast electron density, but not very smaller than it. It should be stressed that this mechanism works by accelerating cold electrons from the gas inwards, and does not work via the outgoing laser-generated fast electrons.

Now we can quantify this idea. Let us assume that the energies of the super-thermal electrons follow a Maxwellian distribution, i.e. $n = n_0 \exp(\phi/T)$ where ϕ is the electrostatic potential and T is the temperature in electron Volts. This can then be used to solve the one dimensional Poisson's equation[20]:

$$\frac{\partial^2 \phi}{\partial x^2} = \frac{q n_h}{\epsilon_0} \exp(\phi/T) \tag{5}$$

which is solved to get the sheath field:

$$E = \frac{E_0}{1 + \frac{x}{\sqrt{2}\lambda_D}} \tag{6}$$

where $E_0 = \sqrt{2 n_h T/\epsilon_0} = 4.3 \cdot 10^{12} V/m$ is the peak electric field strength. As this sheath forms it accelerates electrons from the gas, their final energy being proportional to the integral of the electric field up to that point. However, the integral of equation 6 diverges and so a maximum distance must be enforced. Equation 5 ignores the presence of the gas, adding the gas would, however, reduce the formation of the sheath and so a natural cut-off would be where the density of hot foil electrons is the same as the background gas. By solving equation 5, it can be shown that the electron density in the sheath field is:

$$n = \frac{n_h}{\left(1 + \frac{x}{\sqrt{2}\lambda_D}\right)^2}. \tag{7}$$

The gas density of the electrons is $10^{25} m^{-3} = 0.02 n_h$. Solving equation 7 for x, results in a cut off of about 3.5μm (it was found that the instability that get set up in the gas has a length scale of 4μm which further justifies this cut off). The maximal energy is therefore the integral of equation 6 up to this cut off:

$$W_{eV} = \int_0^{3.5\mu\mathrm{m}} E dx \sim 4.4\mathrm{MeV} \tag{8}$$

which is over double the minimum energy needed for electrons to emit mostly $>$ 100KeV photons. This final value is not too sensitive to small increases in the cut-off value (increasing the cutoff to 4μm increases peak energy to 5.2MeV). For electrons that get accelerated by the sheath field, their final energy is the sum of the kinetic energy gained by acceleration in the sheath and their initial thermal energy, however as the initial temperature was comparatively small in comparison to the typical energies they get accelerated to, (8KeV vs 4.4MeV) the thermal motion can be ignored. It is assumed that all the gas electrons in the sheath get accelerated by the field. As the final energy is just a function of initial position, the energy distribution function can be found via a change of variables:

$$P(W)dW = P(x)\frac{dW}{dx}dx. \tag{9}$$

As the energy is all electrostatic, $E \propto dW/dx$, the distribution function can be found:

$$P(W) \propto \exp(W/2T_h) = \exp(W/2\mathrm{MeV}) \text{ for } W < 4.4\mathrm{MeV} \tag{10}$$

which is plotted in figure 9. In reality the distribution function will be more relaxed than predicted, for example the temporal variations in the sheath field, which have been ignored, will act in such a way that the density at lower energies is higher. As the super-thermal foil electrons follow a Maxwellian distribution, there will exist a proportion with energies above the 4.4MeV cut off and as such, these electrons will not turn around and will travel back through the gas and be lost. Electrons with energies lower than this will recirculate back into the foil, along with the newly accelerated gas electrons. The proportion of electrons which fail to recirculate is:

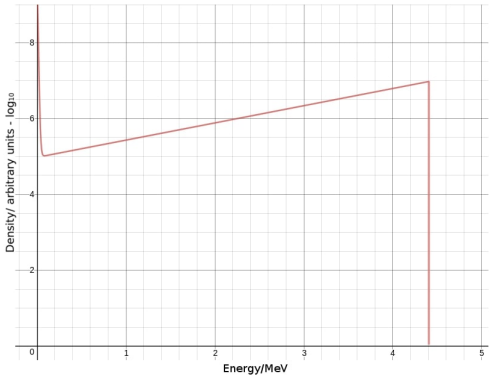

FIG. 9: The predicted distribution function for the accelerated gas electrons. The y axes is plotted on a log scale and the initial thermal energy is included for completeness. Plotted using www.desmos.com

$$\frac{\int_{4.4\mathrm{MeV}}^{\infty} e^{-W/1\mathrm{MeV}} dW}{\int_0^{\infty} e^{-W/1\mathrm{MeV}} dW} \sim 1\%, \tag{11}$$

however, when looking at the high energy ($>$ 2MeV) electrons 10% fail to recirculate. This reduces the average energy of the remaining electron population:

$$\frac{\int_0^{4.4} W e^{-W/1\mathrm{MeV}} dW}{\int_0^{4.4} e^{-W/1\mathrm{MeV}} dW} \sim 0.95\mathrm{MeV}. \tag{12}$$

The following evolution becomes harder to analyse quantitatively. The effect of the prepulse plasma and laser pulse (if the duration is great enough that the pulse is still interacting with the foil when the electrons recirculate back to the front) could have a drastic effect on the front sheath field and hence a drastic effect on the energy distributions of the electrons after they leave and re enter the foil target from the front (laser side) surface. According to the literature[21,22], the distribution function is likely to relax towards a Maxwellian (or Fermi-Dirac distribution) during the transport in the foil, however the strength of such relaxation cannot yet be calculated a priori. It appears more research needs to be conducted before a sufficient understanding is reached to predict what will occur here.

Purely qualitatively it is expected that the above processes will continue with the effects getting less pronounced due to the loss of electrons out the rear of the target and the loss of energy from collisions with the ions in the target (although these are not simulated). Eventually the amount of electrons drawn in from the gas will contribute a sizeable fraction of the total number of super-thermal electrons, this fraction will increase when looking at sub populations at even higher energies.

Studies comparing the energies of emitted protons and electron recirculation for different foil target thicknesses[18,23] conclude that a thinner foil target results in more circulations of the electron. It seems reasonable to conjecture a similar result will occur for increasing the laser pulse duration. A longer laser pulse should also reduce the oscillations of the strength of the sheath field, meaning the drawing in of gas electrons is continuous (and will actually result in more energetic electrons, as all that get drawn in after the initial growth of the sheath will be at the maximum energy).

Throughout this it has been assumed that the ions remain stationary, however as the simulation progresses the sheath field will cause acceleration of the ions[18,19]. This will cause the charge imbalance set up by the electrons leaving the foil at the foil-gas boundary to decrease and hence the sheath field will decrease.

B. Simulations

To analyse the effect, 1D P.I.C simulations were run in *EPOCH*[25]. As the simulations were run in 1D, any effect caused by a non-zero angular spread of electrons will be neglected. Any interaction that occurs at a scale smaller than the step size is also ignored, most importantly this means that the simulations are collisonless[25]. The preliminary test had the following parameters:

- The plasma was quasi-neutral, doubly ionised iron. There was a linear, 5μm prepulse plasma increasing from $n_e = 0$ to $n_e = 10^{28}m^{-3} \approx 6n_c$. The foil target was 15μm long and had a density of $n_e = 6 \cdot 10^{28}m^{-3} \approx 35n_c$. The gas cell was modelled to be 90μm long (the choice here was not physically motivated but motivated by computational time and accuracy) and had a density of $n_e = 10^{25} = 0.006n_c$. The ion density was set as to make the system neutral.

- The electron temperature was set to 8KeV which resulted in a Debye length (in the foil target) of 3nm, which was easily resolved by the set step size of ~ 0.5nm. P.I.C codes often lead to numerical self heating if the Debye length is not fully resolved, hence the need for a lower than physical density and a higher than physical electron temperature. The initial temperature of the ions was set to 0: they are heavy and so any thermal motion can be ignored.

- The laser pulse had a wavelength of 800nm, a Gaussian profile with a FWHM of 36fs and peak intensity of $5 \cdot 10^{19}\mathrm{W/cm}^2$. For the purposes of presenting the results of this 1D simulation, total numbers were calculated assuming a fictitious FWHM diameter of the laser spot set to 5.64μm.

The pulse duration used is considerably shorter than the Vulcan laser pulses used experimentally, however the effect we observe occurs on a much longer time-scale *after* laser irradiation has occurred. These simulations thus demonstrate that the effect is decoupled from the laser-plasma interactions, and that precise replication of the experimental details is not strictly necessary to observe the sheath multiplication mechanism.

170fs after the start of the simulation (the convention will be $t = 0$ refers to the start of the simulation) the laser pulse starts to interact with the prepulse plasma and causes a population of electrons to accelerate, as can be seen in figure 10a. Over the next 80fs the hot electron population travels through the foil and at the foil-gas boundary decelerates and turns back into the foil (figure 10b). The motion then continues back through the foil (figure 10c). At this time the electrons that failed to recirculate are clearly visible and appear to be setting up a disturbance in the gas. The same process happens every time the electron population crosses either the front or rear boundary and so the electrons circulate with a time period of about 120fs, as can be seen by looking at the peak sheath strength (figure 14).

The energy spectrum just before the recirculation occurs (figure 11a) does indeed show a sub population of very fast foil electrons at a temperature of $\sim$ 990KeV. There is, however, also a subpopulation of equally energetic gas electrons already present in the foil; this is caused by an initial, rapid thermal expansion of the gas electrons into the foil, these electrons getting accelerated equally well. This effect is caused by the fact that a gas and a solid are both being modelled as collisionless plasmas and so there is no force to stop the mixing. This thermal expansion should have no noticeable effect: as can be seen, the amount of gas electrons at high energies is a very small fraction ($< 1\%$) of foil electrons at

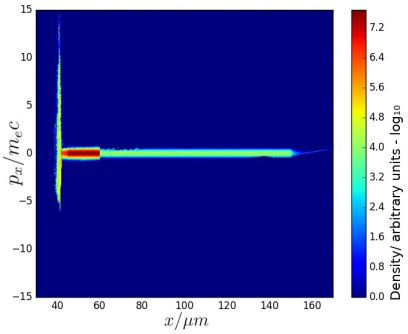

(a)

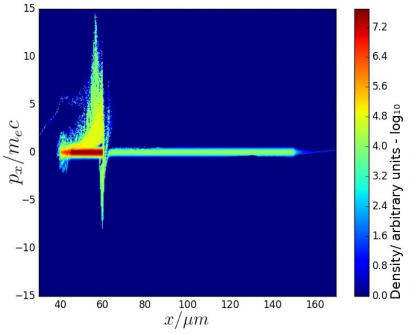

(b)

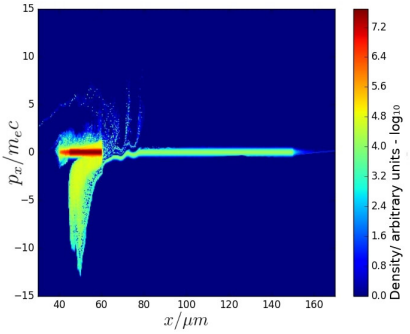

(c)

FIG. 10: Phase space plots: a)the electrons start to be accelerated as the laser hits at $t = 170$fs. b) the electrons reach the rear of the foil at $t = 250$fs and start to circulate back into the foil. c) at $t = 300$fs the electrons are travelling back inside the foil.

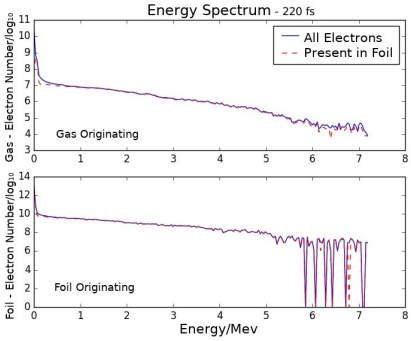

(a)

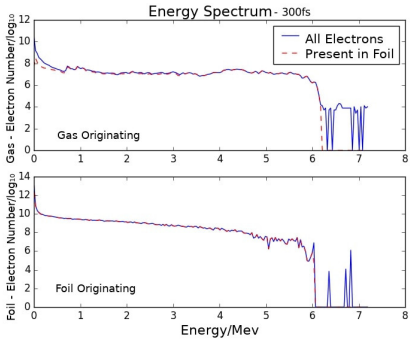

(b)

FIG. 11: Energy spectrum for the gas originating and foil originating electrons for $t = 220$fs (a) and $t = 300$fs (b). The energy spectrum for all of the electrons is plotted in blue and the spectrum for electrons that are in the foil are plotted with red dashes. The cutoff is clearly visible, albeit 50% greater than predicted. In fact, at $250 - 290$fs the distribution function for the gas electrons was closer to that predicted in figure 9.

the same energies. After recirculation at the rear sheath occurs, the amount of high energy electrons that originated in the gas drastically increases (figure 11b). The distribution of such electrons is similar to, but noticeably more relaxed than, the predicted distribution as given in figure 9 and thus provides evidence for the mechanism suggested. The phase space figures (figures 10b and 10c) also clearly show a phase structure connecting the cold gas population with electrons returning into the foil, so the acceleration of cold electrons into the foil is shown directly in the phase space plots.

At around $t = 340$fs the electrons recirculate at the front (laser) side of the foil target. In doing so, the en-

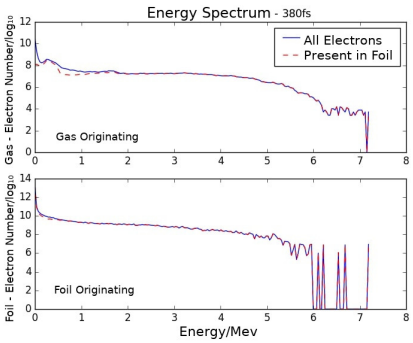

FIG. 12: Energy spectrum for $t = 380$fs.

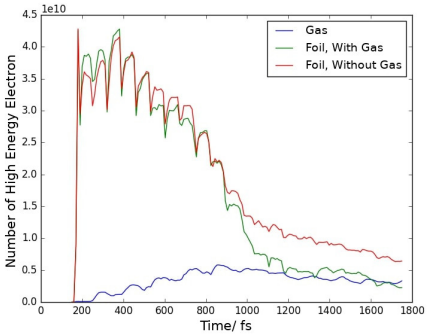

FIG. 13: The number of fast (> 2MeV) electrons active in the simulation split up into those that originated in the gas, those that originated in the foil when the gas was present and those that originated in the foil when it was not.

ergy spectrum appears to relax (comparing the energy spectrum from figure 11b and 12). No calculations have been conducted to analyse this relaxation (either by the authors or found in the literature), more research needs to be done to understand this effect. The simulations showed that, initially, the same number of electrons were accelerated to high temperatures for both cases (with and without gas), as expected, and did not increase beyond this initial maximum. Over time the amount of gas electrons that have been accelerated to high energies increases such that at $t = 900$fs the population of hot gas electrons is 11% of the initial fast electron population, as shown in figure 13. The points where the gradient of the fast gas electron population is greatest, i.e. when the most amount of gas gets accelerated to high energies, occur just after the peak of the sheath field (figure

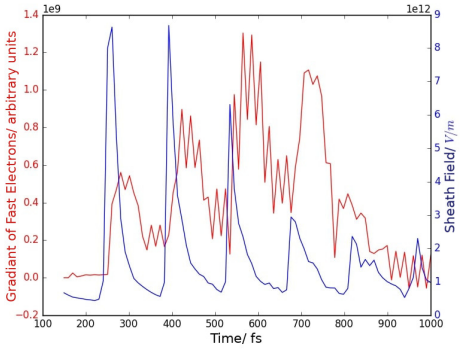

FIG. 14: The gradient ($\propto \frac{dN_{gas}}{dt}$) of the amount of high energy gas electrons and the peak sheath field.

14). This supports the hypothesis that the sheath field is, at least, a major driving force in the acceleration of electrons in the gas.

The temporal decay of the sheath field, and the decline of high energy foil electrons, is most likely caused by the sheath field accelerating the ions in the foil, thus reducing the charge imbalance[19] - energy is taken from the super-thermal electrons and given to the ions. Figure 15 plots the total kinetic energy of the ions and the electrons separately, showing the extent of the energy transfer to the ions. At around a picosecond, the amount of hot electrons, in the gas case, that originated in the foil drops significantly compared to the case without the gas. This phenomenon is most likely a result of the simulation being purely 1D, and thus one must be careful in terms of extrapolating this to actual experiments. However after this time the gas-originating fast electrons become a very significant (>30%) fraction of the fast electron population, at least in this simulation.

The results of these simulations will be sensitive to the gas density. While the gas density is much lower than the fast electron density, any increase in the gas density should result in a roughly linear increase in the number of fast electrons accelerated by this sheath mechanism. As the gas density approaches the fast electron density, we expect the sheath mechanism to become progressively less pronounced. On the other hand, this mechanism is unlikely to be sensitive to factors such as the foil material. The mechanism will depend on any factors in the laser-plasma interaction that affect the fast electron density or temperature.

In summary, the simulations support the hypothesis that the formation of a sheath field at the foil-gas boundary can, in effect, 'multiply' or 'grow' the hot electron population. This is a relatively slow process. The simulations suggest that the magnitude of this effect is at least a 10% increase, but it could be more significant

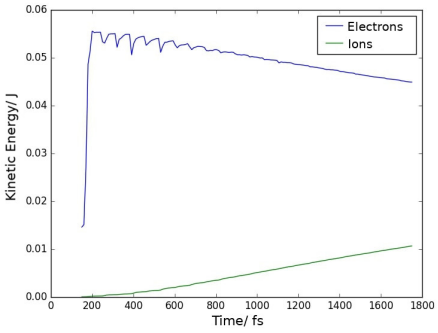

FIG. 15: The total kinetic energy stored in the electrons and the ions. The small oscillations occur when the kinetic energy becomes electrostatic potential energy. Plotted is the case with gas however the case without gas resulted in essentially the same plot; adding the gas did increase the total energy by a few percent, as would be expected from the difference in particle number.

(maybe appoaching a 30% increase). This means that the maximum distortion to the backward to forward x-ray signal due to this mechanism alone would be 1.1–1.3, and this means that the effects reported in Section III are likely to be dominant. Nonetheless it can certainly help contribute to an increase in x-ray emission in these experiments.

V. CONCLUSIONS

This paper summarizes the results of a theoretical investigation motivated by the suspicion that there was enhanced backward x-ray emission in experiments on the VULCAN laser that used gas-cell targets. We have examined two mechanisms that might have contributed to this. The first is natural backward emission of fast electrons. This is strongly supported by 2D PIC simulations and can be plausibly attributed to a combination of the ZVP[26] and DLA[29] mechanisms. The estimated ratio between the backward and forward x-ray emission due to this effect ranges from 1.06 to 3.8, and the experimental observations record ratios in the range of 1.5–3.2, so this is quite consistent with the experimental observations. The second is the 'growth' or 'multiplication' of the hot electron population by the sheath field at the foil-gas boundary. Simulations indicate that the magnitude of this effect might be an increase in the fast electron number between 11–30%, and thus this effect alone can only lead to a signal ratio (backward to forward) of 1.1–1.3 *at most*, which is somewhat low compared to the experimental observations. So it is likely that this mechanism complements and supports the first, or another mechanism. Overall there are at least two mechanisms that can contribute to such an observation, and thus there do appear to be feasible physical mechanisms that could account for this suspicion. We therefore suggest that the physics involved in these gas-cell targets merits further attention.

Perhaps the line of investigation that this study most clearly suggests is to investigate targets that consist of just the foil, the re-entrant cone, and the front wall of the gas cell, i.e. removing the gas. If this studies conclusion regarding the laser-plasma interaction is broadly correct then such a target should reproduce the x-ray emission properties seen in the gas cell experiments. It also is possible that just a conical shell target alone could be sufficient, provided that the cone wall thickness and material is sufficient to act as effective bremsstrahlung convertor.

ACKNOWLEDGEMENTS

The authors are grateful for computing resources provided by STFC's Scientific Computing department. All data used to produce the figures in this work can be made available upon request to the authors.

[1] Wood, J.C. , Chapman,D.J., Poder,K., Lopes, N.C., Rutherford, M.E., White,T.G., Albert,F., Behm,K.T., Booth,N., Bryant,J.S.J., Foster,P.S., Glenzer,S., Hill,E., Krushelnick,K., Najmudin,Z., Pollock,B.B., Rose,S., Schumaker,W., Scott,R.H.H., Sherlock,M., Thomas,A.G.R., Zhao,Z., Eakins,D.E. & Mangles,S.P.D., Sci. Rep. 8, 11010 (2018)

[2] C M Brenner, S R Mirfayzi ,D R Rusby ,C Armstrong ,A Alejo, L A Wilson ,R Clarke,H Ahmed ,N M H Butler ,D Haddock ,A Higginson,A McClymont , C Murphy ,M Notley ,P Oliver , R Allott , C Hernandez-Gomez,S Kar , P McKenna ,D Neely, Plasma Phys. Control. Fusion, 58, 014039 (2015)

[3] C. D. Armstrong, C. M. Brenner, C. Jones, D. R. Rusby, Z. E. Davidson, Y. Zhang, J. Wragg, S. Richards, C. Spindloe, P. Oliveira, M. Notley, R. Clarke, S. R. Mirfayzi, S. Kar, Y. Li, T. Scott, P. McKenna, and D. Neely, High Power Laser Science and Engineering, 7, E24 (2019)

[4] Borghesi, M., Campbell, D. H., Schiavi, A., Willi, O., MacKinnon, A.J., Hicks, D., Patel, P., Gizzi, L.A., Galimberti, M., Clarke, R.J. 2002, Laser and Particle Beams, 20, 641

[5] Borghesi, M., Bulanov, S., Campbell, D. H., Clarke, R.J., Esirkepov, T.Zh., Galimberti, M., Gizzi, L.A., MacKinnon, A.J., Naumova, N.M., Pegoraro, F., Ruhl, H., Schiavi, A., Willi, O., 2002, Physical Review Letters, 88, 135002

[6] Osterhoff, J., Popp, A., Major, Z., Marx, B., Rowlands-Fees, T.P., Fuchs, M., Geissler, M, Horlein, R., Hidding, B., Becker, S., Peralta, E.A., Schramm, U., Gruner, F., Habs, D., Krausz, F., Hooker, S.M., Karsch, S., 2008, Physical Review Letters, 101, 085002

[7] Ahmed, H., Dieckmann, M. E., Romagnani, L.,Doria, D., Sarri, G., Cerchez, M., Ianni, E., Kourakis, I., Giesecke, A.L., Notley, M., Prasad, R., Quinn, K., Willi, O., Borghesi, M., 2013, Physical Review Letters, 110, 205001

[8] Ahmed, H., Doria, D., Dieckmann, M. E., Sarri, G., Romagnani, L., Bret, A., Cerchez, M., Giesecke, A.L., Ianni, E., Kar,S., 2017, The Astrophysical Journal Letters, 834, L21

[9] Private communication with R.J. Clarke CLF STFC

[10] Roberts, K. V., & Berk, H. L. 1967, Physical Review Letters, 19, 297

[11] Laguitton, D., & Parrish, W. 1977, X-ray Spectrometry, 6, 201

[12]Woan, G. (2000) The Cambridge Handbook of Physics Formulas. Cambridge: Cambridge University Press.
[13]Gibbon, P. (2005). Short Pulse Laser Interactions with Matter: An Introduction. London: Imperial College Press.
[14]Mulser, P., & Bauer, D. 2010, American Institute of Physics Conference Series, 1308, 6
[15]Davies, J. R. 2009, Plasma Physics and Controlled Fusion, 51, 014006
[16]Wilks, S. C., Kruer, W. L., Tabak, M., & Langdon, A. B. 1992, Physical Review Letters, 69, 1383
[17]Huang, Y.-s., Lan, X.-f., Duan, X.-j., Tan, Z.-x., Wang, N.-y., Shi, Y.-j., Tang, X.-z., He, Y.-x., 2007, Physics of Plasmas, 14, 103106
[18]Sentoku, Y. 2002, APS Meeting Abstracts, FI2.002
[19]Hatchett, S. P., Brown, C. G., Cowan, T. E., Henry, E.A., Johnson, J.S., Key, M.H., Koch, J.A., Langdon, A.B., Lasinski, B.F., Lee, R.W., MacKinnon, A.J., Pennington, D.M., Perry. M.D., Phillips, T.W., Roth, M., Sangster, T.C., Singh, M.S., Snavely, M.S., Stoyer, M.A., Wilks, S.C., Yasuike, K., 2000, Physics of Plasmas, 7, 2076
[20]Dendy, R.O & Ham, C.J. An Introduction to High Temperature Plasma Physics. In preparation.
[21]Levin, Y., Pakter, R., & Teles, T. N. 2008, Physical Review Letters, 100, 040604
[22]Kadomtsev, B. B., & Pogutse, O. P. 1970, Physical Review Letters, 25, 1155
[23]MacKinnon, A. J., Sentoku, Y., Patel, P. K., Price,D.W., Hatchett,S.,Key,M.H., Andersen,C., Snavely,R., Freeman,R.R., 2002, Physical Review Letters, 88, 215006
[24]Boyd, T.J.M.& J.J. Sanderson, 2003. The Physics of Plasmas. 1st ed. Cambridge: Cambridge University Press.
[25]Arber, T. D., Bennett, K., Brady, C. S., Lawrence-Douglas, A., Ramsay, M.G., Sircombe, N.J., Gillies, P., Evans, R.G., Schmitz, H., Bell, A.R., Ridgers, C.P, 2015, Plasma Physics and Controlled Fusion, 57, 113001
[26]Baeva, T, Gordienko, S, Robinson, APL, Norreys, PA 2011 Phys. Plasmas, **18**, 056702
[27]Savin, AF, Ross, AJ, Serzans, M, Trines, RMGM, Ceurvorst, L, Ratan, N, Spiers, B, Bingham, R, Robinson, APL, Norreys, PA, 2017, Phys. Plasmas, **24** 113103
[28]https://physics.nist.gov/PhysRefData/Star/Text/ESTAR.html
[29]Robinson, APL, and Arefiev, AV 2018, Phys. Plasmas, **25**, 053107
[30]Fonseca, R.A., Silva, L.O., Tsung, F.S., Deckyk, V.K., Lu, W., Ren, C., Mori, W.B., Deng, S., Lee, S., Katsouleas, T., Adam, J.C. , 2002, Lecture Notes in Computer Science, **2331**, 342-351

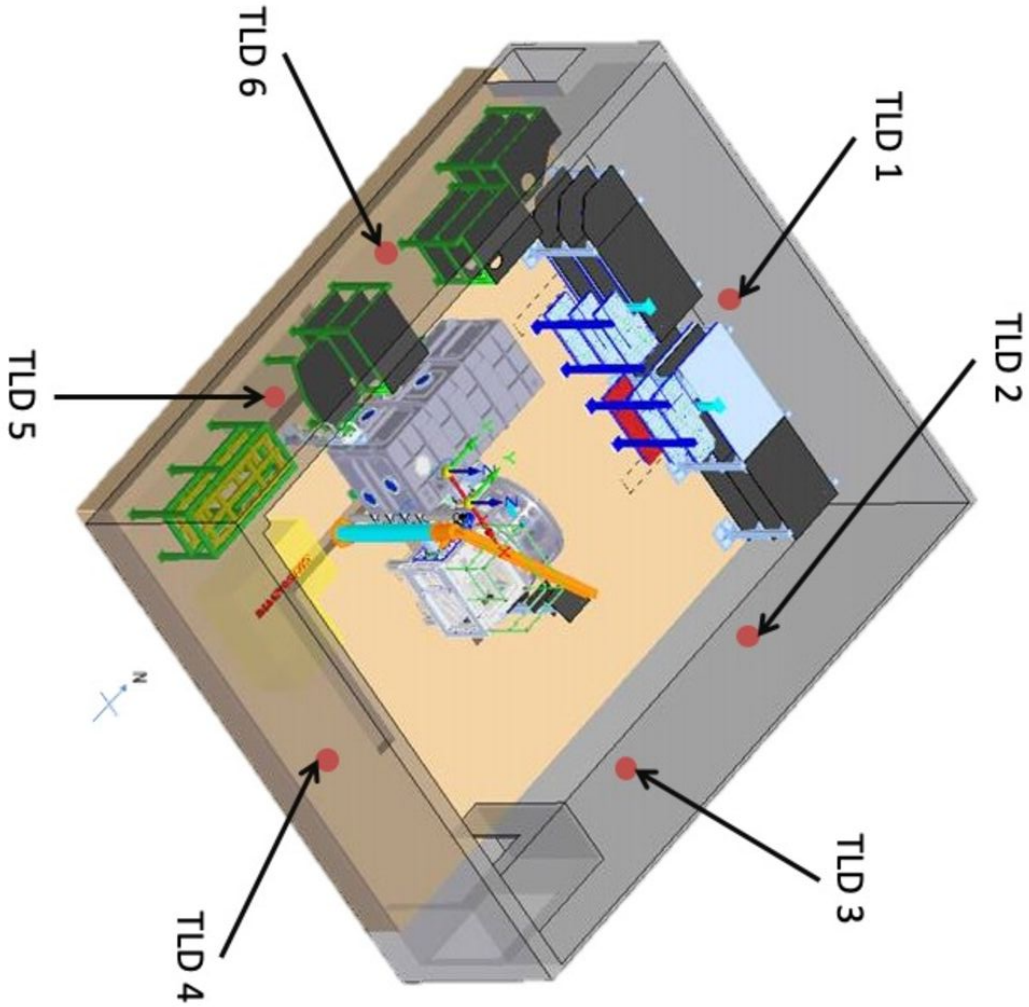

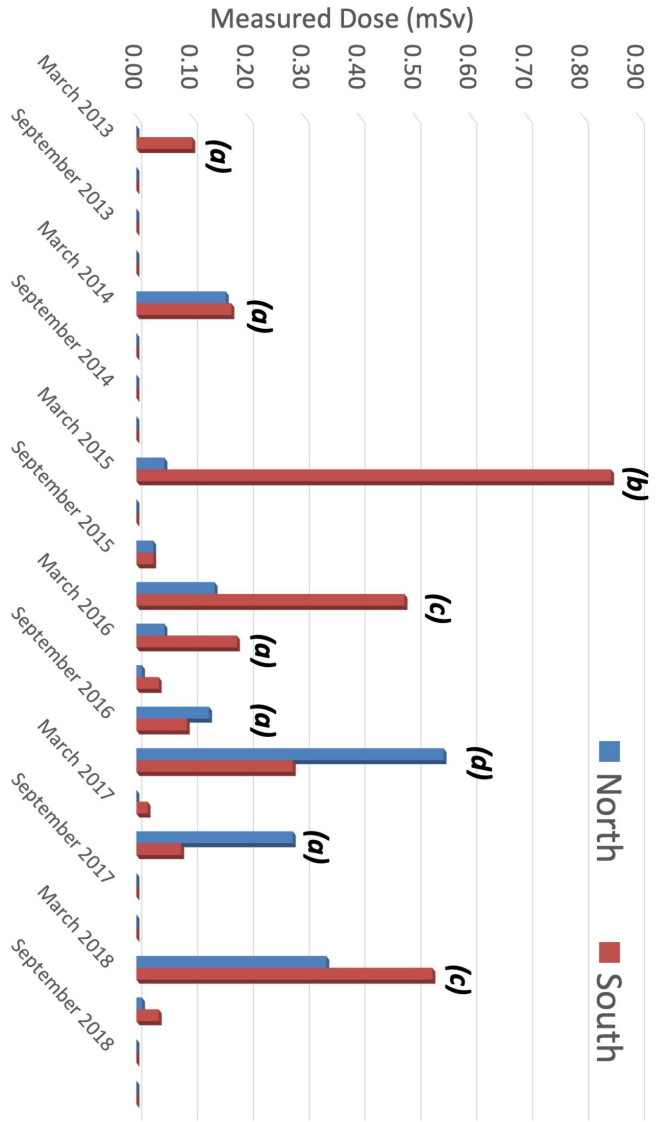

PLEASE CITE THIS ARTICLE AS DOI: 10.1063/5.0021221

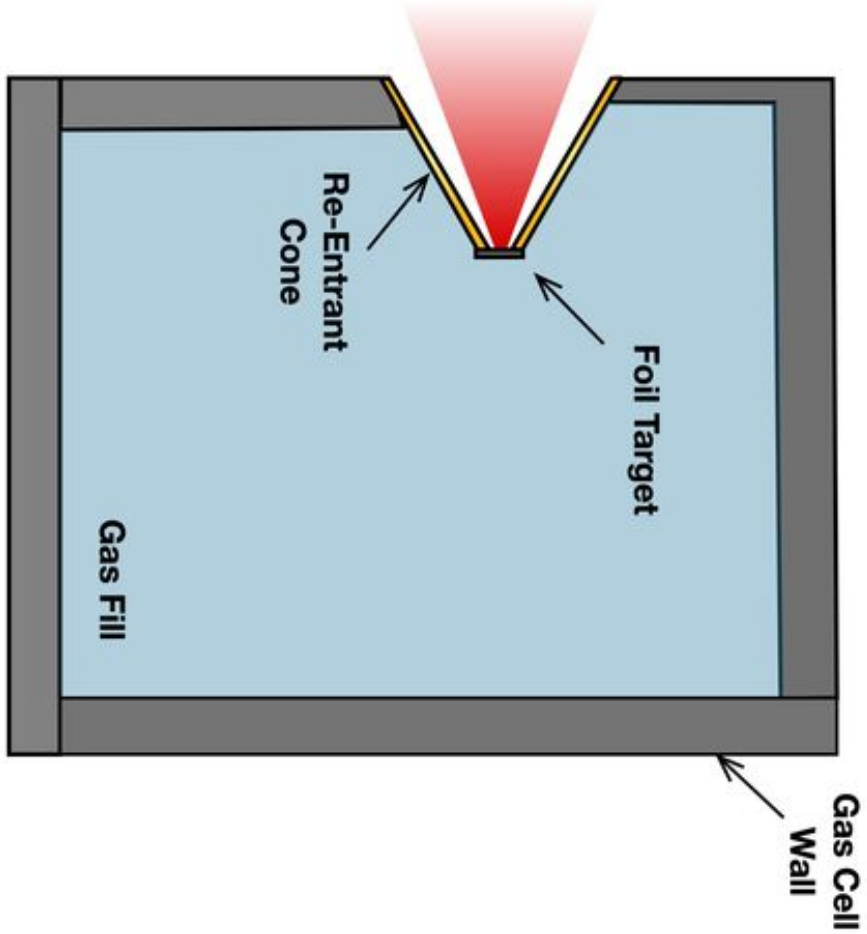

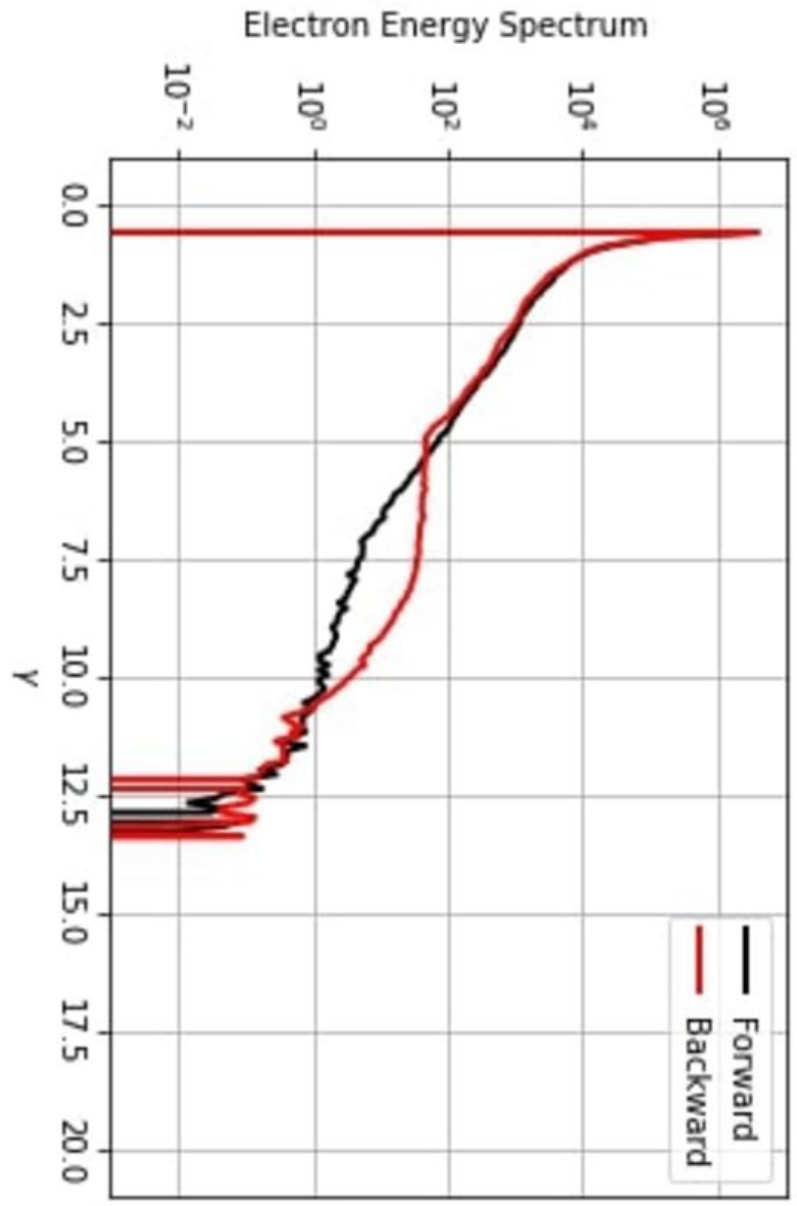

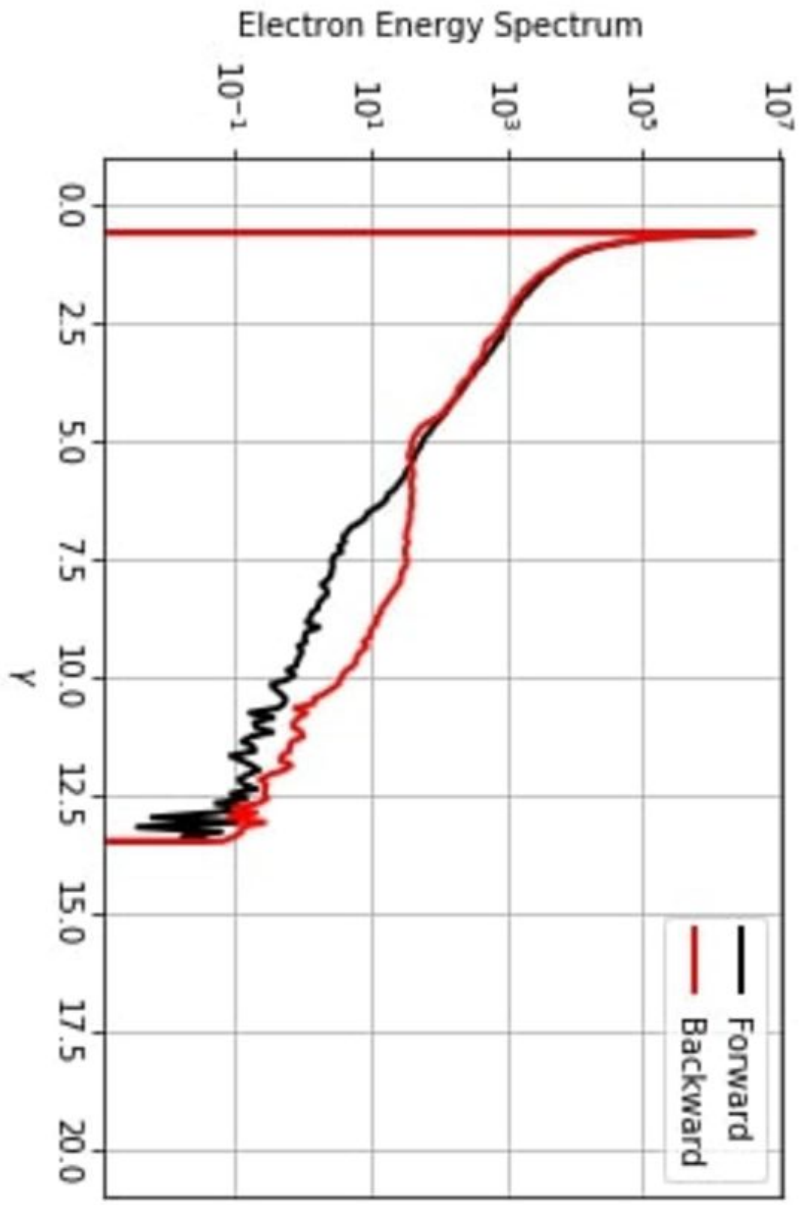

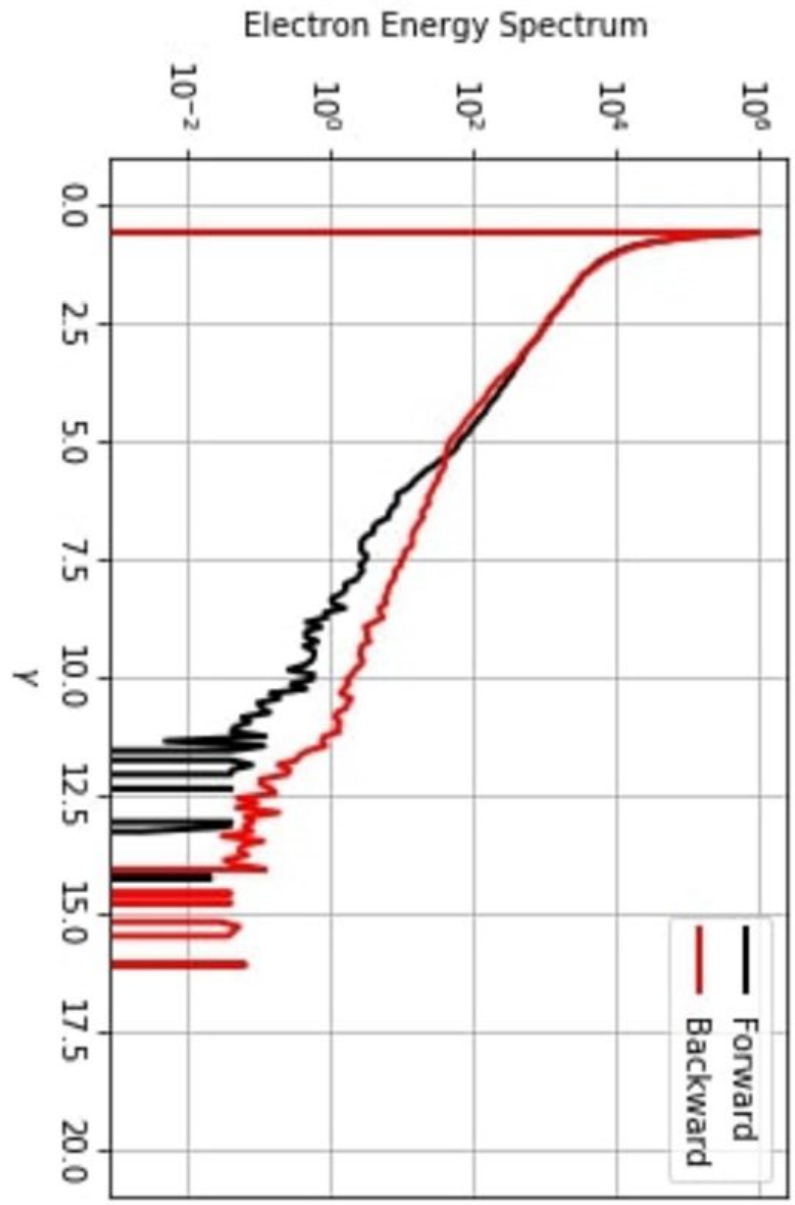

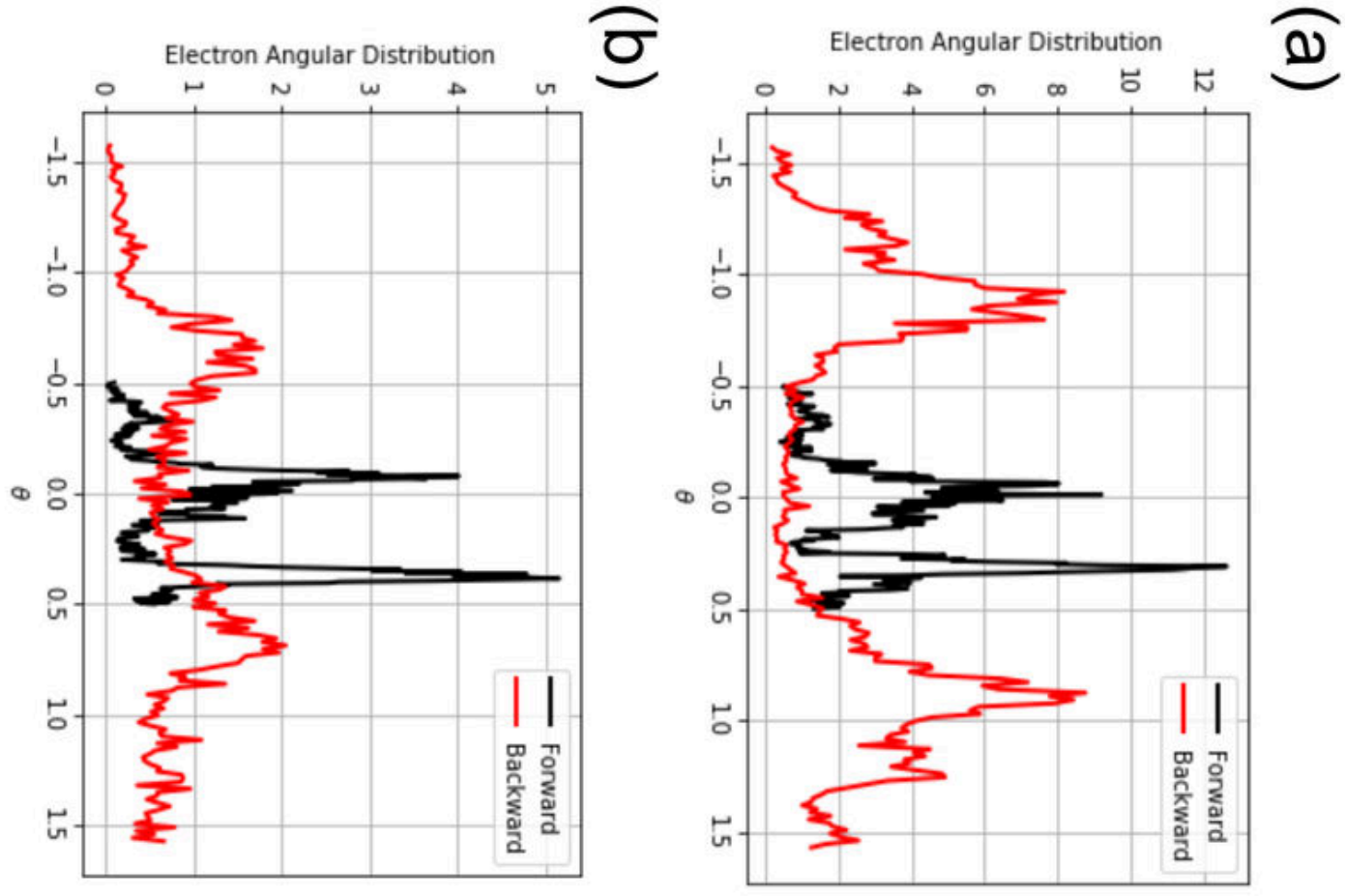

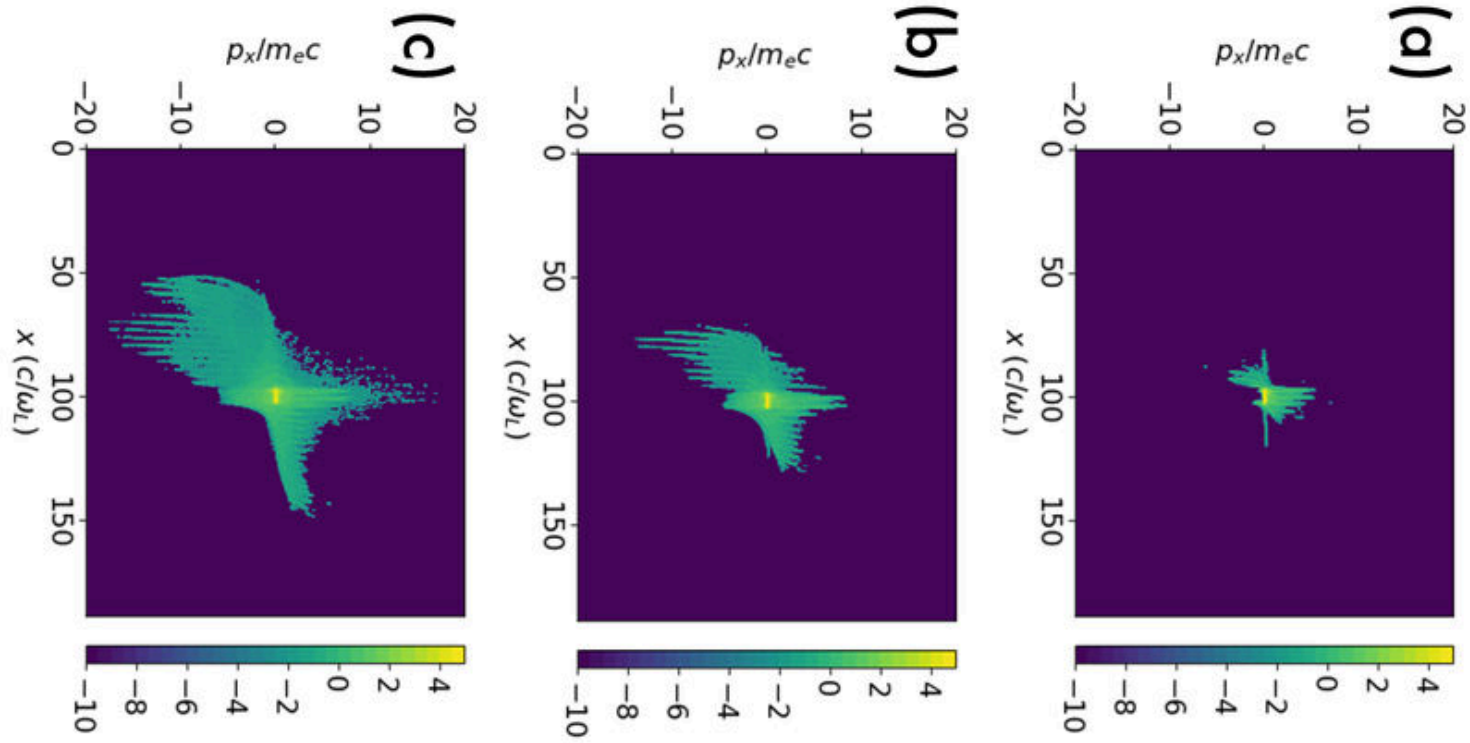

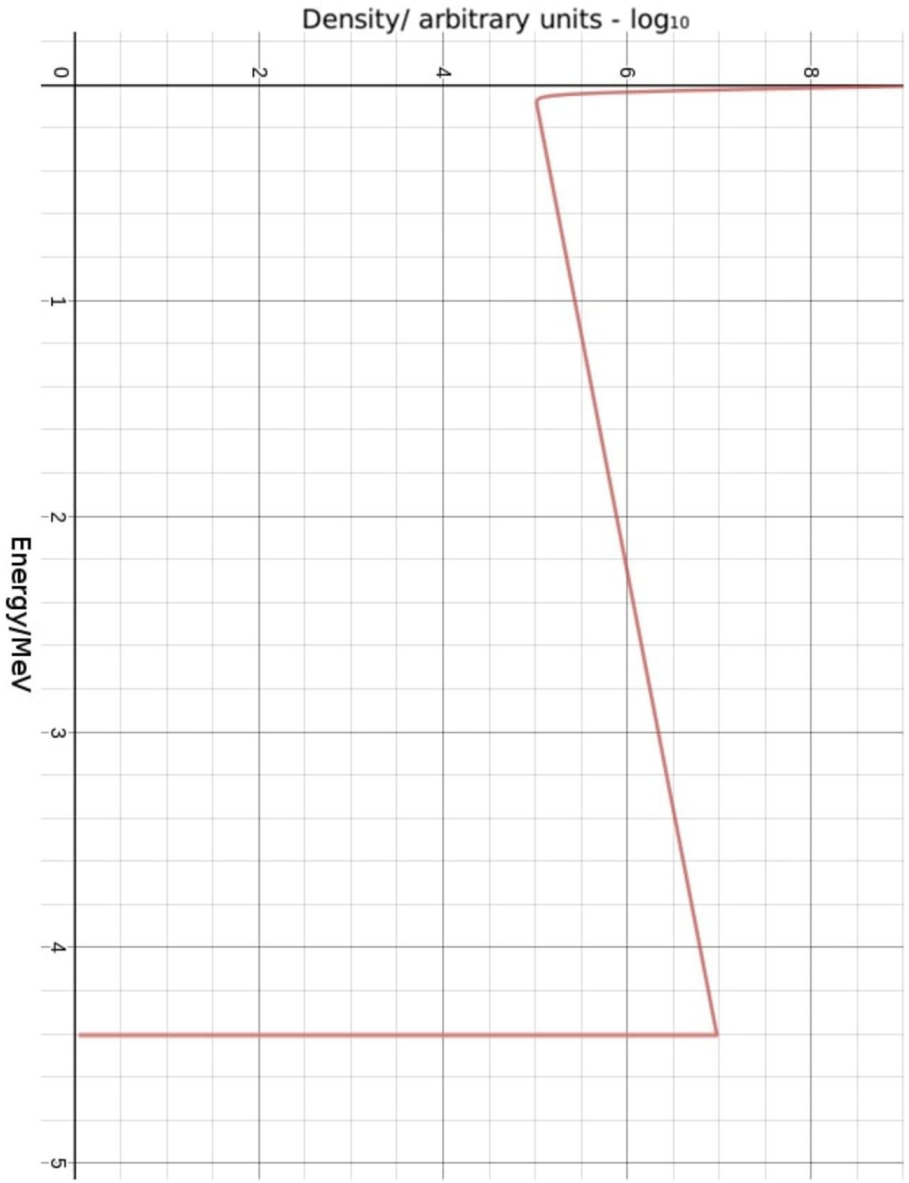

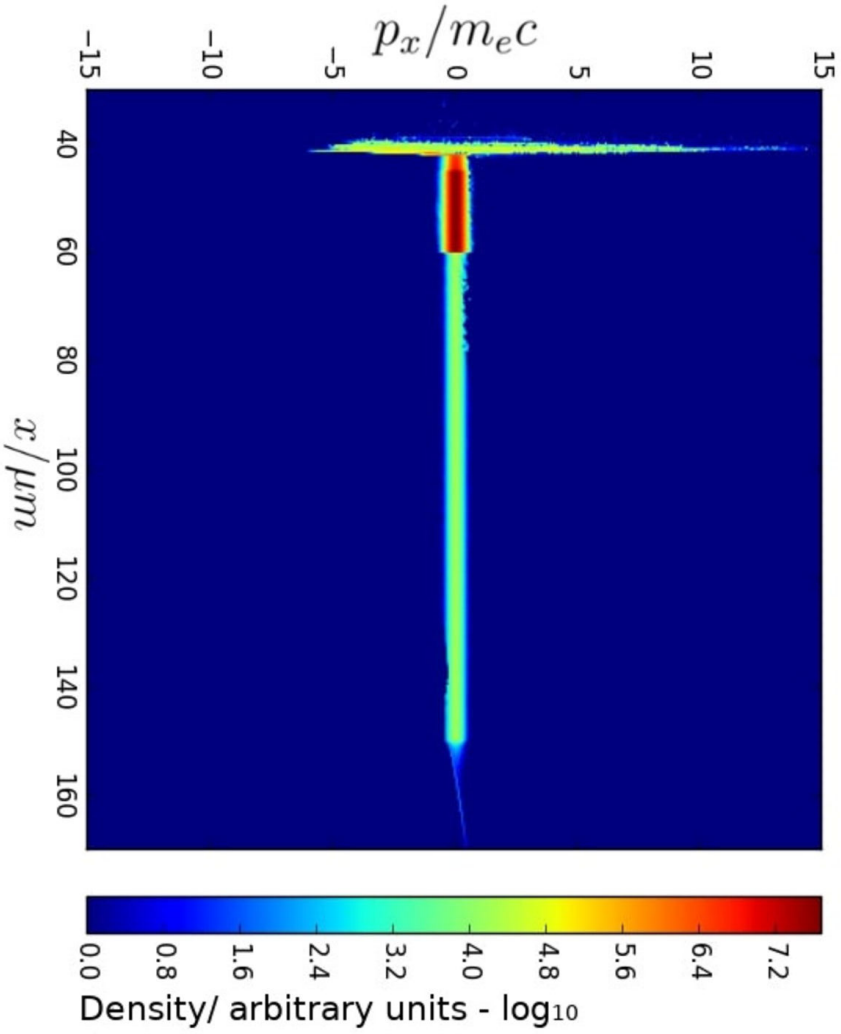

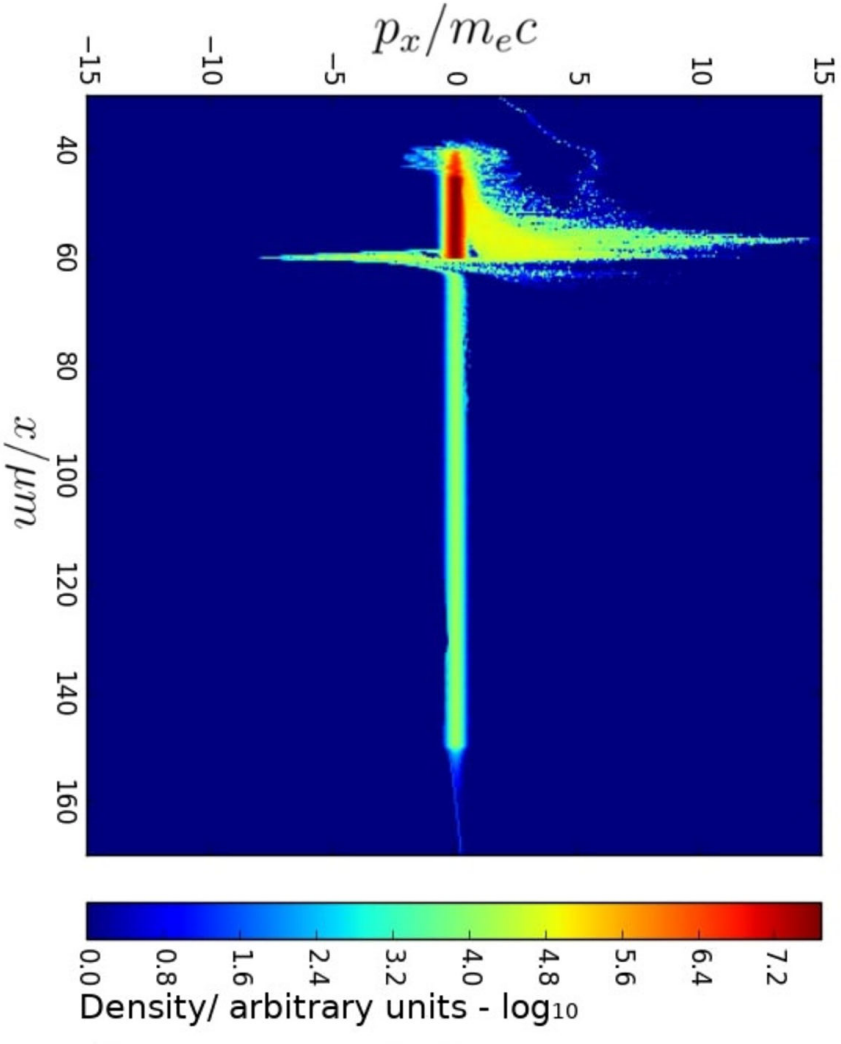

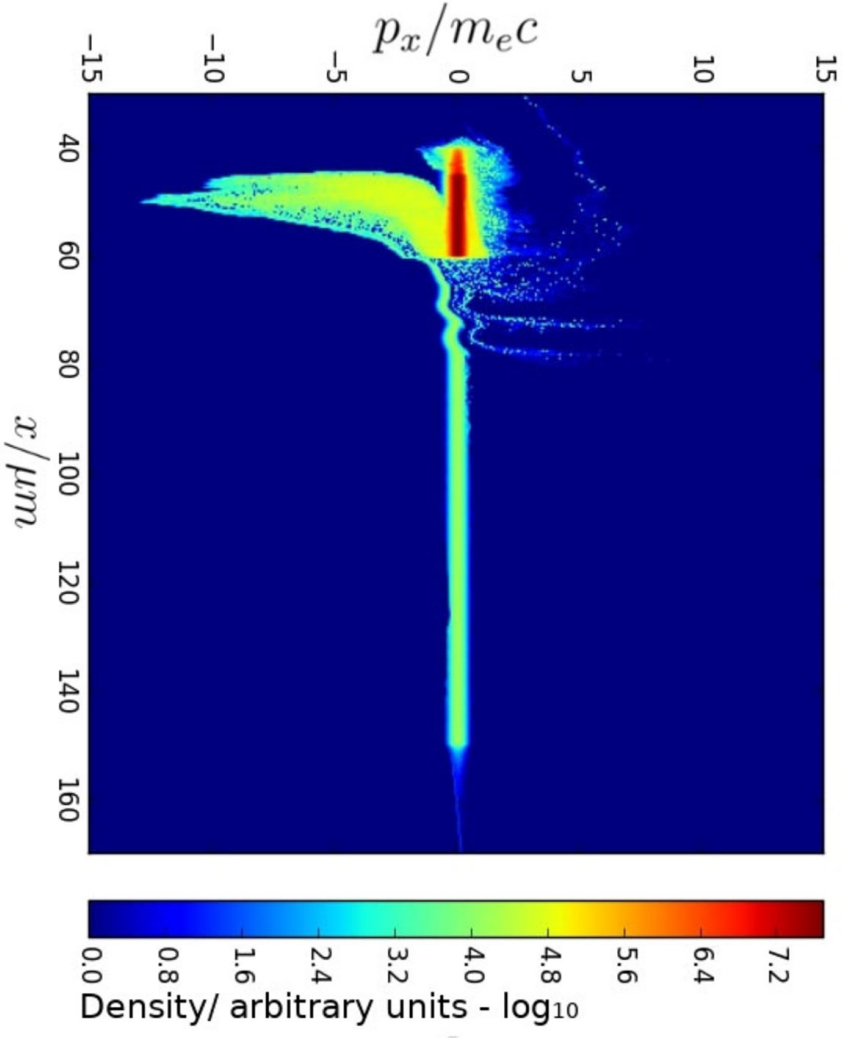

PLEASE CITE THIS ARTICLE AS DOI: 10.1063/5.0021221